

# Thalamic interneurons and relay cells use complementary synaptic mechanisms for visual processing

Xin Wang<sup>1,3</sup>, Vishal Vaingankar<sup>1</sup>, Cristina Soto Sanchez<sup>1</sup>, Friedrich T Sommer<sup>2</sup> & Judith A Hirsch<sup>1</sup>

Synapses made by local interneurons dominate the thalamic circuits that process signals traveling from the eye downstream. The anatomical and physiological differences between interneurons and the (relay) cells that project to cortex are vast. To explore how these differences might influence visual processing, we made intracellular recordings from both classes of cells *in vivo* in cats. Macroscopically, all receptive fields were similar, consisting of two concentrically arranged subregions in which dark and bright stimuli elicited responses of the reverse sign. Microscopically, however, the responses of the two types of cells had opposite profiles. Excitatory stimuli drove trains of single excitatory postsynaptic potentials in relay cells, but graded depolarizations in interneurons. Conversely, suppressive stimuli evoked smooth hyperpolarizations in relay cells and unitary inhibitory postsynaptic potentials in interneurons. Computational analyses suggested that these complementary patterns of response help to preserve information encoded in the fine timing of retinal spikes and to increase the amount of information transmitted to cortex.

Inhibitory neurons dominate the intrinsic circuits of the lateral geniculate nucleus of the thalamus. Specifically, the neurons that project to cortex, relay cells, rarely form local contacts<sup>1</sup>; instead, most intranuclear connections derive from local interneurons<sup>2,3</sup>. Even the earliest recordings from relay cells emphasized that inhibition seemed stronger in thalamus than in retina<sup>4</sup>. The inhibition is powerful; it can determine whether relay cells fire tonically or in bursts<sup>5,6</sup>, sharpen visual selectivity<sup>4</sup> and otherwise influence input to cortex. However, there is scant knowledge of how thalamic inhibitory circuits operate during vision. We combined whole-cell recording and labeling *in vivo* with visual stimulation and computational analyses to explore how local interneurons process sensory information.

Relay cells have receptive fields that comprise a concentric center and surround<sup>4</sup> with push-pull responses to stimuli of the opposite contrast (for example, where bright stimuli excite, dark stimuli inhibit<sup>5,7</sup>). This arrangement can be explained by a circuit in which retinal cells supply direct excitation via monosynaptic connections and indirect inhibition through local interneurons<sup>2,8</sup>. Accordingly, our results showed that interneurons have receptive fields with a center-surround organization and even have push-pull responses. Also, the responses of interneurons, similar to those of relay cells<sup>9</sup>, could be approximated with simple computational models. Thus, one might assume that all thalamic receptive fields are built the same way, as appears to be the case for excitatory and inhibitory cells in visual cortex<sup>10,11</sup>.

Steadily accumulating evidence, however, suggests that thalamic relay cells and interneurons have profoundly different anatomical and physiological attributes. For example, ganglion cells synapse with the proximal

dendrites of relay cells, but favor the distal processes of interneurons<sup>8</sup>, where active currents help to boost excitation<sup>12</sup>. Furthermore, relay cells communicate through conventional axonal contacts, whereas both dendrites and axons of local interneurons synapse onto target cells<sup>8,13</sup>.

We found that these differences between cell types were reflected by markedly distinct visual responses. For relay cells, preferred stimuli evoked large, unitary excitatory postsynaptic potentials (EPSPs), and nonpreferred stimuli elicited graded inhibition. The picture for interneurons was the inverse; excitation was smooth, whereas inhibitory responses comprised jagged trains of unitary inhibitory postsynaptic potentials (IPSPs). The rates and receptive fields of both types of unitary events were consistent with a feedforward origin.

The difference between signals could, in principle, be explained by differences in anatomical connectivity<sup>8,13–16</sup> and membrane properties<sup>12,17</sup>. Moreover, computational and theoretical analyses suggested that the inverted forms of excitation and inhibition work in concert to transmit precise temporal information from the periphery to cortex. As much of the structure of thalamic circuits is conserved across species and modalities<sup>14,18</sup>, it is likely that our results illustrate a fundamental property of sensory processing.

## RESULTS

We made whole-cell recordings from 119 cells in 22 adult female cats, 1.5–4.5 kg and sampled the main layers, A, A1 and C, of the lateral geniculate. We were able to stain 36 neurons, including 27 relay cells and 9 interneurons<sup>19–21</sup>. These and the remaining cells were also classified by physiological criteria (see below).

<sup>1</sup>Department of Biological Sciences and Neuroscience Graduate Program, University of Southern California, Los Angeles, California, USA. <sup>2</sup>Redwood Center for Theoretical Neuroscience, University of California, Berkeley, Berkeley, California, USA. <sup>3</sup>Present address: Computational Neurobiology Laboratory, The Salk Institute for Biological Sciences, La Jolla, California, USA. Correspondence should be addressed to J.A.H. (jhirsch@usc.edu).

Received 16 September; accepted 21 October; published online 19 December 2010; doi:10.1038/nn.2707

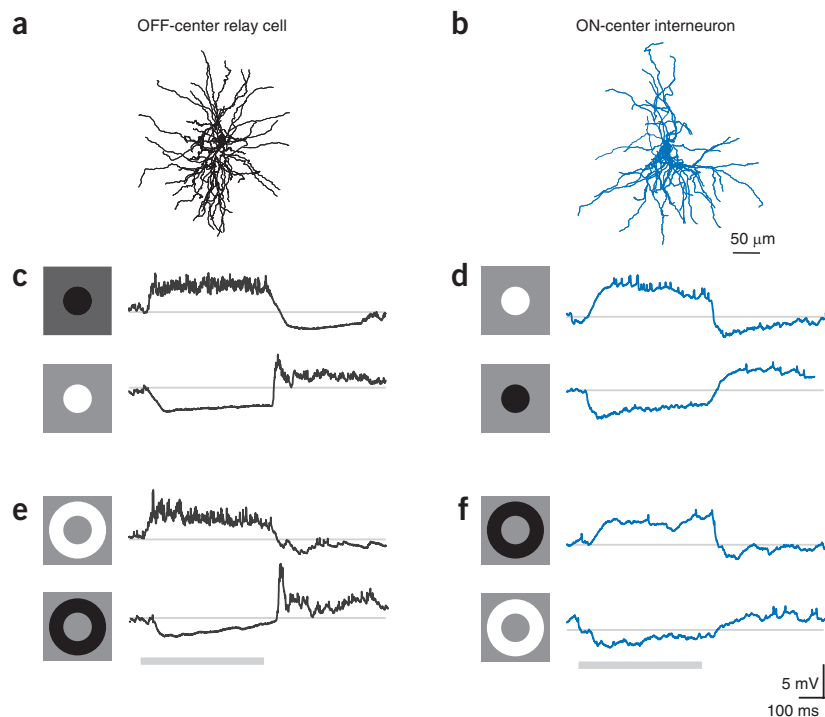


**Figure 1** Push-pull responses of an OFF-center relay cell and ON-center interneuron.

(a) Anatomical reconstruction of an OFF-center relay cell. (b) Reconstruction of the dendrites of an ON-center interneuron (the axon was too pale to trace continuously). (c, d) Averaged responses of the membrane voltage to dark and bright disks flashed in the center of the receptive field in the relay cell (c) and the interneuron (d). The icons on the left depict stimulus shape and contrast. (e, f) Averaged responses of the membrane voltage to annuli flashed in the surround of the receptive field in the relay cell (e) and interneuron (f). The gray line under the traces marks the stimulus duration in c–f.

stimulus to generate spatiotemporal receptive fields shown as contour plots (Fig. 2a) alongside the time course for the peak pixel for four cells (Fig. 2b), an ON and an OFF relay cell and an ON and an OFF interneuron (note, Gaussian noise lacks spatial coherence and high contrasts and so drove far stronger responses from the center than the surround). The spatial and temporal components of the response were similar for all cell types.

Next, we built standard linear-nonlinear cascade models. The linear stage was the response-triggered average of the stimulus (effectively, the receptive field) for which we substituted averages of the membrane current for the conventional spike rate. The second stage was a nonlinearity that mapped the output of the linear filter to the strength of response<sup>24</sup>; the nonlinearity was fit with a sigmoidal function (Fig. 2c), although a linear fit performed almost as well.

We then streamed a novel noise sequence (different from that used for the model) through the model and plotted the result against the actual prerecorded response to the novel stimulus (Fig. 2d). The model predicted the responses of all cells to the same extent, as measured by explained variance (Fig. 2e). Thus, to a first approximation, the synaptic receptive fields of both relay cells and interneurons appeared to be similar in shape and explanatory power. Note that the explained variance here (roughly 40%) was less than that achieved by past extracellular studies. This is likely because intracellular signals have far more complicated, effectively ‘noisier’, shapes than spikes and also because we used a long stimulus sequence, which precluded presentation of multiple repeats<sup>5</sup>. Furthermore, we could not characterize other aspects of the response, such as the contrast gain, to furnish additional parameters for better fits<sup>25</sup>. All told, responses to disks and annuli and to dense noise suggested that the receptive fields of relay cells and interneurons were similar.

### Correlating intracellular waveform with cell class

So far we have described averaged responses to visual stimuli. We next analyzed the intracellular records at a finer grain to learn how receptive fields are built. We found that relay cells and interneurons processed feedforward drive in stereotypically different ways.

We investigated the structure of neural responses by recording during the presentation of various types of visual stimuli. We used voltage-clamp mode rather than current-clamp mode to reduce the influence of intrinsic membrane conductances on synaptic input<sup>5</sup>. The membrane currents recorded from most cells (~75%) were dominated by trains of prominent excitatory postsynaptic currents (EPSCs; Fig. 3a and refs. 5,26). We anatomically identified 27 of 89

### Distribution of excitation and inhibition in the receptive field

The most basic question that we asked was whether the receptive fields of interneurons resembled those of relay cells (Fig. 1a–f). Relay cells have receptive fields that consist of a center and surround in which stimuli of the reverse contrast evoke responses of the opposite sign<sup>5</sup>. Dark disks flashed in the center of an OFF (X type) relay cell (Fig. 1a) drove excitatory responses (Fig. 1c), whereas bright disks evoked hyperpolarization (Fig. 1c), as illustrated by averaged records of the membrane voltage following repeated trials of the stimulus. The equivalent situation held for responses to annuli flashed in the surround (Fig. 1e). The excitation, or push, is almost certainly fed forward from retinal ganglion cells of the same center sign<sup>22,23</sup>. A simple explanation for the pull is that it comes from interneurons that also have receptive fields with a center-surround structure, but have the opposite preference for stimulus contrast (Supplementary Fig. 1a and ref. 5).

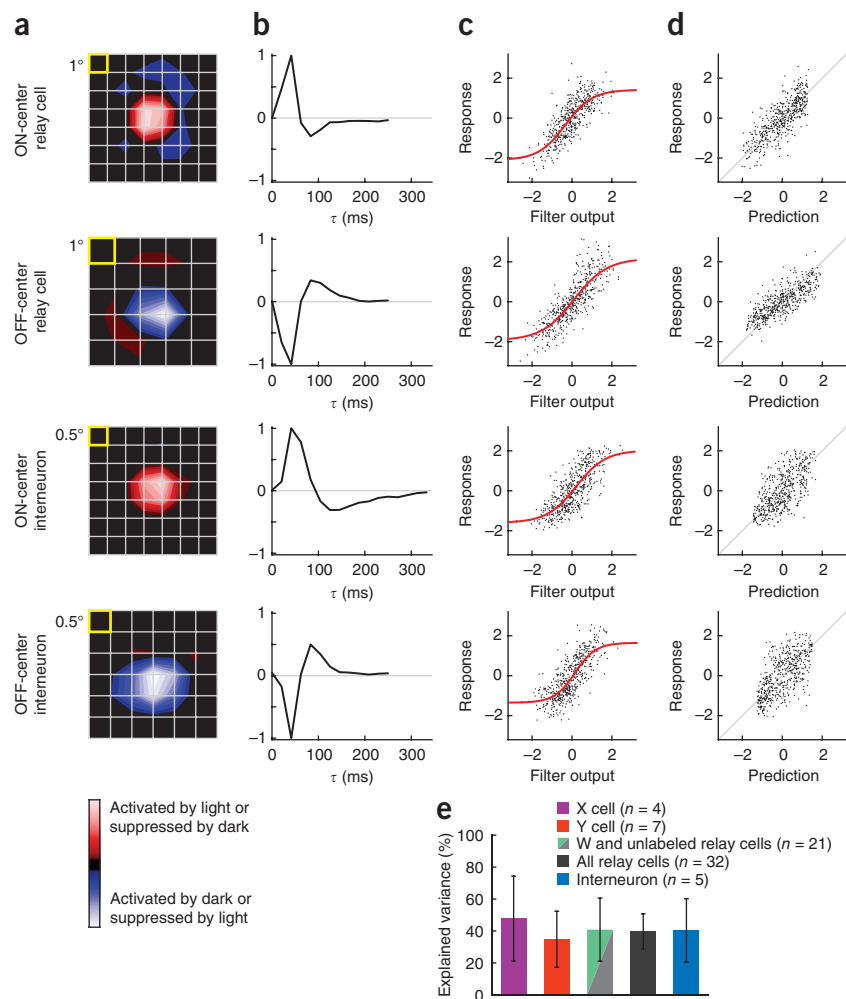
Consistent with this scheme, we found that interneurons had receptive fields with a center-surround structure (Fig. 1d,f), as illustrated for an ON interneuron (Fig. 1b). Moreover, there was a push-pull arrangement of responses in each subregion; bright stimuli in the ON center or dark stimuli in the OFF surround were excitatory, whereas stimuli of the opposite contrast were inhibitory (Fig. 1d,f). Notably, the excitatory response of this particular interneuron rose more slowly than that of the relay cell; however, this might not indicate a trend for the population (Fig. 2).

### Quantitative assessments of receptive fields

Disks and annuli drive the center and surround strongly; they were useful for visualizing spatially opponent excitation and inhibition. The next step was to compare the synaptic responses of relay cells and interneurons quantitatively at higher spatial resolution. For this analysis, we used Gaussian white noise<sup>24</sup>.

Past studies of relay cells have employed simple linear-nonlinear models to characterize neural responses<sup>24</sup>. We extended this approach to interneurons, using reverse correlation of synaptic responses to the

**Figure 2** Receptive fields of relay cells and interneurons and prediction of neural responses using linear-nonlinear models. **(a,b)** Spatial **(a)** and temporal **(b)** receptive fields of two relay cells and two interneurons computed from the intracellular response (see ref. 5). Stimulus size is indicated by the yellow box. **(c)** Scatter plots of the actual intracellular response against that obtained using a linear filter made from the spatiotemporal receptive field show how the nonlinear component (red curve) of the model was fit. **(d)** Comparison of the actual and predicted responses. The actual response was normalized so that the mean was zero and the variance was unity. **(e)** Performance of the model, quantified by explained variance for populations of relay cells ( $n = 32$ ) and interneurons ( $n = 5$ ). Error bars represent s.d.



neurons from which recordings were made; all were relay cells, including X, Y and W subclasses<sup>5,26</sup>. This observation was not surprising, as retinal inputs produce prominent EPSPs<sup>27</sup>; in contrast, events generated by corticothalamic neurons are typically invisible unless the membrane resistance is increased with drugs<sup>28</sup>.

The recordings obtained from the remaining cells (~25%) were markedly different. The most salient components were brief, net hyperpolarizing currents that were often preceded by depolarizing transients from which the occasional spike escaped (Fig. 3b). We labeled 9 of 30 cells with this physiological profile and found that all were interneurons (Online Methods and Supplementary Fig. 2). Thus, there was a qualitative distinction between the two waveforms; one was characterized by unitary depolarizing currents and the other by unitary hyperpolarizing currents. This difference held true for stimuli as diverse as Gaussian noise and natural movies<sup>5,26</sup>.

To quantify the difference between the waveforms, we devised a metric called the deflection index (Online Methods and Supplementary Fig. 3), which measured the asymmetry in the inward versus outward deflections of the membrane current over different timescales. The values of the index were positive when the membrane trajectory was hyperpolarizing and were negative for depolarizing excursions. Plots made by measuring the value of the index from short to long intervals for single cells (Fig. 3c) confirmed the impression made by eye (see Fig. 3a,b). The curves for the (labeled and putative) interneurons peaked at a positive value and those for the (labeled and putative) relay cells peaked at a negative value. We then used principal component analysis to characterize the structure of these curves and found that data were divided into two separate modes (Fig. 3d). Furthermore, statistical calculations of conditional probability showed that the physiological profile predicted anatomical class with high fidelity (Online Methods).

### Voltage dependence of membrane currents

It seemed unlikely that the disparity between waveforms merely reflected levels of membrane polarization. Our recordings (Figs. 1 and 3) were usually made at holding levels above the reversal for inhibition and just below the threshold for firing to visualize excitatory

and inhibitory input (see Figure 1 in ref. 5). Furthermore, one class of response never switched to the other. Also, we usually recorded both types of responses in a single experiment (19 of 22), sometimes one immediately after the other, suggesting that the difference between waveforms did not correlate with particular animals or physiological states.

To assess the voltage dependence of the intracellular waveforms, we made recordings from single cells while injecting different amounts of depolarizing and hyperpolarizing current. As anticipated for EPSPs, the inputs recorded from the majority population (labeled and putative relay cells) grew larger as the membrane became more hyperpolarized (Fig. 4a). In contrast, the unitary events recorded from the minority population (labeled and putative interneurons) reversed sign when the membrane was made progressively negative, as expected for events dominated by IPSPs (Fig. 4b,c). Thus, the disparity between the shapes of the unitary events seemed to reflect different types of synaptic input.

From these analyses (Figs. 3 and 4), we concluded that relay cells and interneurons can be classified on the basis of synaptic response. Thus, we refer to cells with intracellular currents dominated by EPSCs as being relay cells and those with records dominated by inhibitory postsynaptic currents as being interneurons.

Are there other physiological characteristics that distinguish relay cells from interneurons? Previous work *in vitro* found that interneurons often have thinner action potentials than relay cells<sup>29</sup> but that the distribution of widths overlap<sup>29</sup>. We did not attempt to measure spike width at half height, as the high-frequency components of

**Figure 3** Quantitative comparison of postsynaptic currents recorded from all cells. **(a,b)** Examples of membrane currents characteristic of relay cells in black **(a)** and interneurons in blue **(b)** recorded in response to Gaussian noise (top) or natural movies (bottom) for four different cells. **(c)** Normalized deflection indices plotted against time scale for the whole dataset ( $n = 119$ ); darker, thicker curves are from neurons illustrated in **a** and **b**. **(d)** Histogram plotting the distribution of the first principal component of the deflection index measured for each cell.

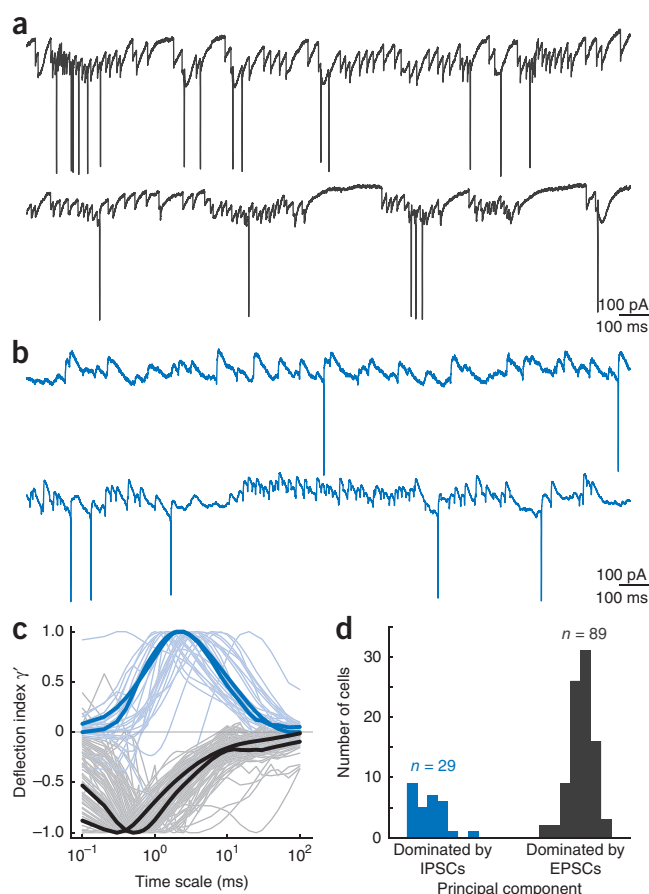
the intracellular signals were often filtered (see ref. 10). Similarly, the general shapes of bursts fired at anode break seem different for feline relay cells and interneurons<sup>29</sup> but might be too variable for quantitative comparison.

### Visual modulation of different types of synaptic inputs

How do the different patterns of synaptic input that we have illustrated (Figs. 3 and 4) sum to create the push-pull responses depicted as averages (Fig. 1)? To address this question, we analyzed individual responses to dark and bright disks. For relay cells, the push (excitation) was made from trains of EPSCs. This pattern is illustrated by responses of an OFF cell to dark disks (Fig. 5a). Conversely, the pull (inhibition) evoked by bright disks was graded (Fig. 5a). The situation for the interneurons was inverted. The push was so smooth that depolarizing synaptic events could not be resolved (Fig. 5b). In contrast, the pull was made by rapid trains of inhibitory events (Fig. 5b; see also Supplementary Fig. 4 for examples of individual responses of an interneuron recorded in current-clamp mode).

The receptive fields of all of the unitary excitatory and inhibitory events had a center-surround structure, as if driven by retinal afferents. We asked whether the unitary events shared another feature with ganglion cells, sustained fast rates<sup>30,31</sup> (corticothalamic neurons have slow rates<sup>32</sup>). We detected unitary events before, during and after the disks were flashed in the center of the receptive fields (Online Methods and Fig. 6). The range in sustained event rates (measured during the second half of the stimulus interval) for excitatory stimuli was 0.8–9.2 ( $4.1 \pm 3.8$ , mean  $\pm$  s.d.) events per s for interneurons and 40.3–184.3 ( $112.2 \pm 65.5$ ) events per s for relay cells. The range for suppressive stimuli was 34.2–76.9 ( $54.5 \pm 17.3$ ) events per s for interneurons and 0.0–38.2 ( $8.2 \pm 16.8$ ) events per s for relay cells.

The event rates for some relay cells (Fig. 6a,b) were faster than those for others and for all of the interneurons. These higher rates likely represent convergent retinal input<sup>22,23,33</sup>. Accordingly, an expanded segment of the trace (Fig. 6b) revealed large and small EPSCs that were probably generated by more than one ganglion cell. These results suggested that both types of unitary events track retinal input.



### Distribution of receptive fields in visual space

Anatomical studies have shown that relay cells and interneurons populate the full extent of the lateral geniculate<sup>2,3,34</sup>. Thus, one would expect that the two types of responses should appear at all retinotopic positions. We assessed the distribution of the receptive fields of both types of cells across visual space by marking their positions (relative to the area centralis) on a tangent screen. The range of occurrence for relay cells (Fig. 7a,b) and interneurons (Fig. 7c,d) were similar and covered most of the geniculate. The inferior and superior locations that seem undersampled correspond to only small slivers of tissue. Thus, the two types of processing that we describe were a ubiquitous feature of the nucleus.

### Modeling different patterns of synaptic integration

We used an exponential leaky integrate-and-fire model to explore how the distinct forms of synaptic integration that we have described might influence the quality and quantity of information that relay cells transmit downstream. The parameters of the model were based on intracellular recordings<sup>35,36</sup> and on evidence that most relay cells receive input from multiple interneurons (for example, see ref. 37)

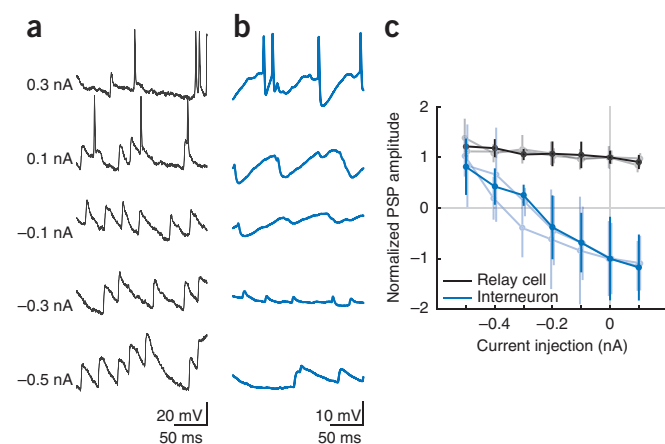
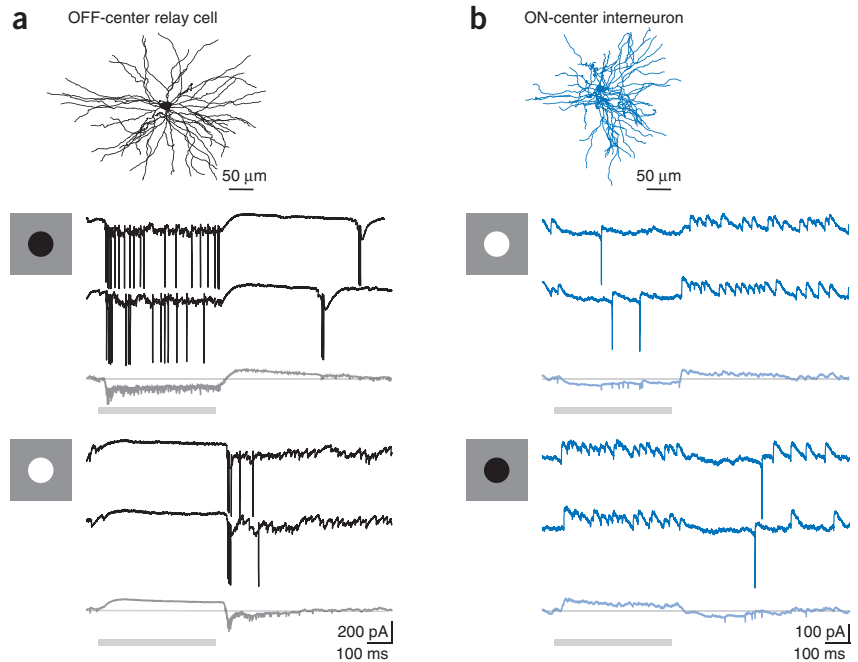


**Figure 4** Voltage dependence of postsynaptic potentials recorded from relay cells and interneurons. **(a,b)** Spontaneous inputs to a relay cell **(a)** and interneuron **(b)** recorded while different amounts of current were injected, as indicated at left. **(c)** Averaged amplitudes of PSPs as a function of current injection, normalized to PSP amplitude at rest for three relay cells and three interneurons. Error bars indicate the s.d. Darker lines indicate responses shown in **a** and **b**. Records from relay cells are in black and from interneurons in blue.

**Figure 5** Visual modulation of synaptic inputs to relay cells and interneurons. (a,b) Responses to disks of the preferred and anti-preferred contrast flashed in the centers of the receptive field of an OFF-center relay cell (a, black) and interneuron (b, blue). The dendritic arbors of each cell are drawn above responses to two individual presentations of the stimulus (darker colors) and the average for all trials (lighter colors). Gray bars indicate stimulus duration.



but are dominated by one retinal afferent (for example, see ref. 23). The signal that drove the model had statistics based on natural scenes (pink noise) and was mediated by excitatory (AMPA) and inhibitory (GABA<sub>A</sub>) conductances driven in a push-pull pattern.

We compared the results of three different versions of the model using information theory to quantify how efficiently the sensory signal was encoded by the relay cell's spike train (Fig. 8). The control model simulated the actual pattern of jagged excitation and smooth inhibition that we recorded from relay cells (Fig. 8b,c). For the remaining two models, we altered the pattern of synaptic response either by smoothing excitation (Fig. 8b,c) or by using jagged inhibition (Fig. 8b,c and Online Methods).

The first question we asked was how each different condition influenced the transmission of information across varied timescales. Our simulations showed that the effect of smoothing excitation was to reduce the information rate density in the millisecond range (Fig. 8d); that is, this quantity fell far below control values when spike times were measured with high temporal precision. The total amount of information conveyed per unit time at fine timescales was

reduced as well (Fig. 8e). Altering inhibition by replacing smooth with jagged IPSCs also had a deleterious effect. This manipulation decreased the information transmitted across all timescales (Fig. 8e) because it disrupted temporal relationships between retinal inputs and the spikes they evoked from relay cells. We then estimated the total rate of information that the relay cell transmitted in each of the three cases. The control simulations yielded substantially higher rates than either test case (Fig. 8f). All told, the results of our simulations suggest that jagged excitation is important for relaying temporally precise information, whereas smooth inhibition improves the transfer of information overall.

## DISCUSSION

Our results provide, to the best of our knowledge, the first intracellular analysis of how local interneurons in the lateral geniculate nucleus of the thalamus encode visual stimuli. Previous studies of relay cells had shown that bright and dark stimuli flashed in the center or surround of the receptive field evoke responses of the opposite sign<sup>5</sup>. This push-pull pattern is most easily explained by direct excitation from the retina and indirect inhibition routed through local interneurons (Supplementary Fig. 1a). Consistent with this scheme, we found that receptive fields of local interneurons resembled those of relay cells. Despite this similarity, the synaptic inputs recorded from the two types of cells during visual stimulation had almost inverted shapes. Excitatory stimuli evoked rapid sequences of unitary excitatory events in relay cells, but elicited relatively smooth and graded depolarizations in interneurons.

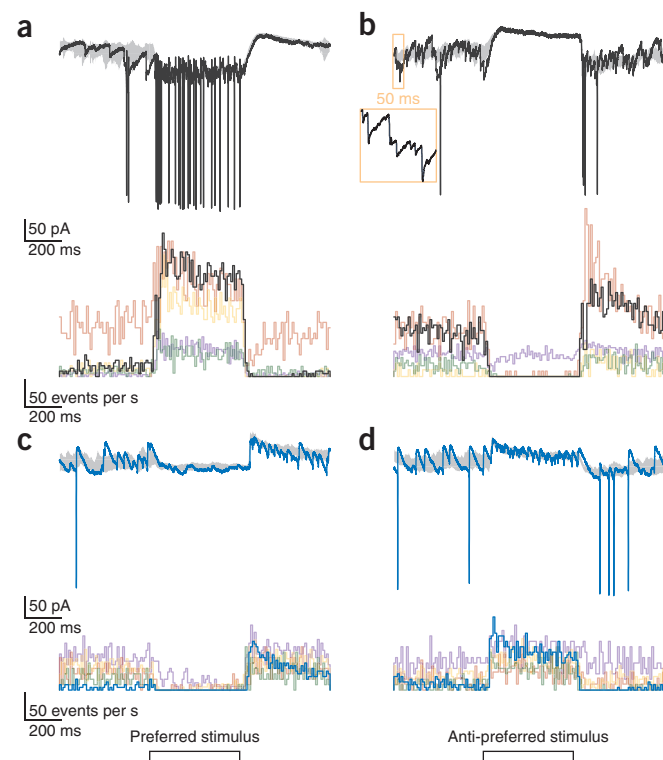


**Figure 6** Rates of unitary synaptic events recorded from relay cells and interneurons. (a,b) Responses to disks of the preferred (a) and anti-preferred (b) contrast flashed in the center of the receptive field of a relay cell (example trial, black; variance across trials, gray) shown above histograms of EPSC rates for the same (black) and four additional relay cells (different colors). Bin size is 5 ms. Inset shows a segment of the recording at an expanded timescale and doubled gain to reveal differently sized EPSCs. (c,d) Companion responses and plots of event rate for five interneurons.

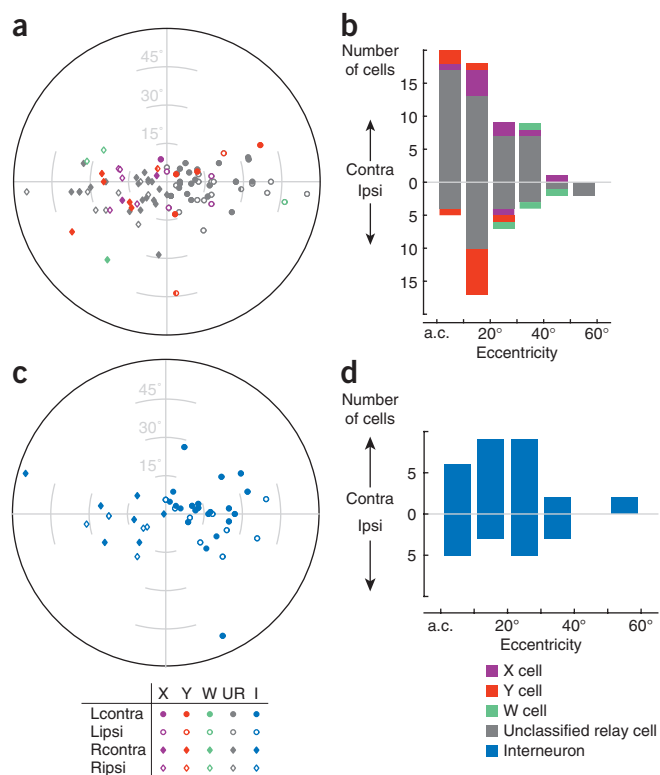


**Figure 7** Spatial distribution of relay cells and interneurons. (a–d) Spatial distribution of the receptive fields of relay cells (a,b) and interneurons (c,d) shown as polar plots (a,c) and frequency histograms (b,d). a.c., area centralis.

Conversely, suppressive stimuli elicited smooth and graded inhibition in relay cells but elicited rapid trains of unitary inhibitory events in interneurons. The rates and receptive fields of both types of unitary events appeared to be inherited, directly or indirectly, from retinal ganglion cells. Thus, the high-frequency components of afferent activity were retained in the excitatory responses of relay cells but were low-pass filtered in the inhibitory responses and vice versa for interneurons. Simulations based on our recordings suggest that these different patterns of response work together to preserve the fine temporal structure of retinal activity and to transmit information effectively.

### Receptive field structure of interneurons

Earlier extracellular studies of the thalamus suggest that all cells in the main layers of the geniculate have receptive fields with a center-surround structure<sup>20,21,33,38,39</sup>. Our analyses moved beyond these studies in two essential ways. First, we were often able to stain cells and link receptive field structure with morphological class. Second, as intracellular recording gives view of subthreshold inputs, we were able to show that interneurons and relay cells alike had a push-pull arrangement of excitation and inhibition in the center and the surround.

Push-pull in a single neuron extends the dynamic range of operation and speeds responses to reversals in stimulus polarity. These effects might be amplified when presynaptic cells also have push-pull responses. For example, interneurons would alternately inhibit or disinhibit their targets as luminance contrast changes from the nonpreferred to the preferred. The presence of push-pull is also seen in retina and in (the cat's) cortical layer 4 (refs. 7,11); hence, it appears to be a basic principle for constructing neural circuits in the early visual pathway.

We do not wish to give the impression that interneurons and relay cells have identical receptive fields and response properties. For example, the two types of cells might differ in adaptation to contrast and/or luminance<sup>25</sup>. In addition, as interneurons receive many more retinal synapses than relay cells<sup>2,3</sup>, they might have larger receptive fields; our current sample is too small to address this issue. Furthermore, we did not recover labeled cells in the interlaminar zones, suggesting that we did not record there.

### Patterns of synaptic input that build receptive fields

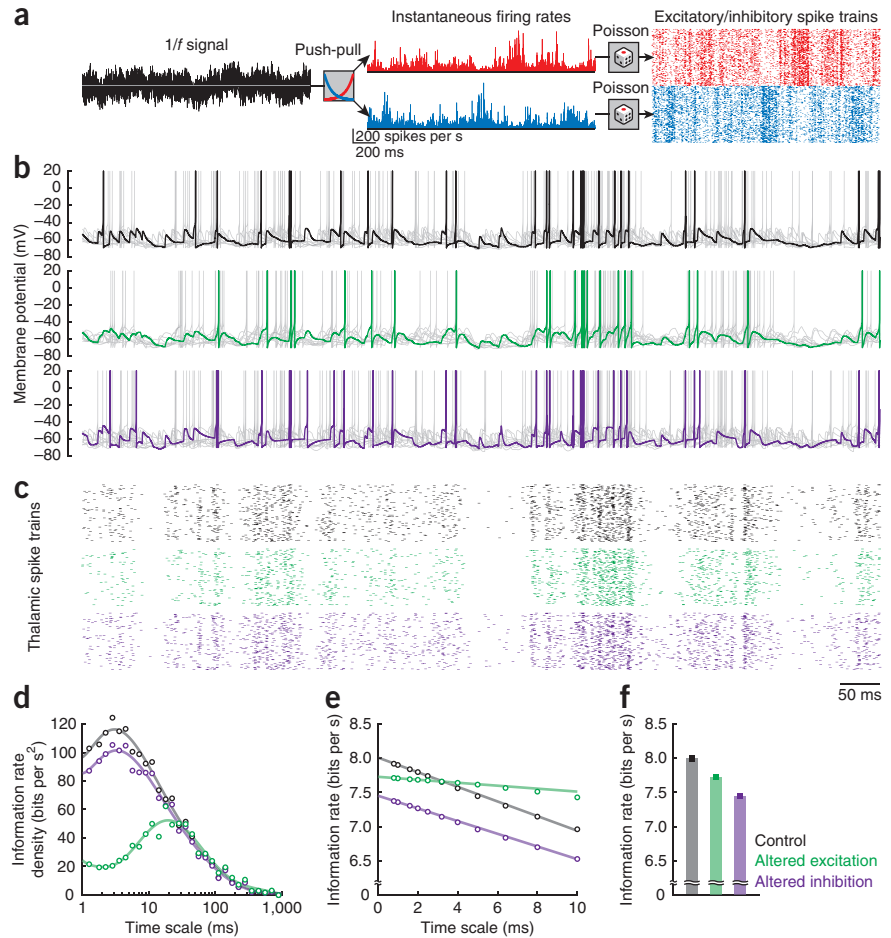
The membrane currents recorded from the lateral geniculate were divided between two different types of waveforms. This dichotomy did not reflect somatic versus dendritic recording sites, as electrode tracks confirmed that patches were made at or near the soma. Nor did the divide correlate with presence or absence of triads; records from all relay cells were similar (triads involve synaptically coupled dendrites of two cells, an interneuron and either a relay cell (commonly X type) or a second interneuron, that are innervated by a single retinal bouton<sup>8,13,40</sup>). Instead, the disparities in waveform correlated with relay cells versus interneurons.

Before we made this observation, it seemed likely that relay cells and interneurons were wired in similar ways. This idea was based, in part, on our past studies of the input layer of the cat's cortex, which showed that excitatory and inhibitory cells not only had indistinguishable receptive fields but also seemed to use comparable patterns of synaptic integration<sup>10,11</sup>. That is, it was impossible to discriminate one type of cortical cell from the other based on subthreshold patterns of response. However, contrary to our initial expectations, we found that the synaptic origins for push-pull responses in thalamic relay cells and interneurons were different.

The unitary synaptic inputs that provide the main excitatory drive, or push, to relay cells almost certainly derive from retina. These inputs have the prominent size and stereotyped shapes of retinogeniculate EPSPs<sup>5,26,36</sup> and also preserve the fast rates and receptive field structure of ganglion cells<sup>30,31</sup>. Why, then, should unitary retinal inputs to interneurons be difficult to detect *in vivo*? Cable models show that retinal inputs to interneurons are often electrotonically remote and might attenuate before reaching the soma if dendrites were passive<sup>41</sup>. However, recent work has shown that retinal input activates dendritic L-type calcium currents that prevent attenuation by propagating excitation over long distances<sup>12</sup>. Thus, either proximal or distal retinal inputs might be masked by the intrinsic conductances that they evoke<sup>12</sup>. In addition, summation of multiple retinal inputs<sup>2,3,12</sup>, as well as metabotropic components of the synapse<sup>17</sup>, could further smooth the time course of feedforward drive. Finally, local collaterals of relay cells might supplement retinal inputs<sup>1,42,43</sup> by providing disynaptic feedforward excitation.

For relay cells, we hypothesize that the pull, or inhibitory response to stimuli of the opposite contrast, derives from local interneurons whose pooled input<sup>8</sup> averages to generate a graded signal, perhaps with a contribution from the perigeniculate nucleus<sup>44</sup>. Local interneurons also have strong pull responses, but these are built by serial hyperpolarizing deflections that have the fast maintained rates typical of ganglion cells<sup>30,31</sup>. A brief depolarizing notch often preceded each deflection, indicating an excitatory component. We can only speculate about the underlying circuitry. We describe one idea that takes the rate and shape of the deflections into account and is consistent with ultrastructural evidence showing that interneurons not only receive substantial input from the retina<sup>2,3</sup>, but also form dendrodendritic synapses with each other<sup>14,45</sup>. We illustrate this idea using an ON interneuron whose push is generated by presynaptic ON

**Figure 8** Simulations of information transmitted by circuits that use different forms of synaptic integration. **(a)** Inputs to an exponential leaky integrate-and-fire model of a thalamic relay cell. A pink ( $1/f$ ) noise signal (left) is transformed by complementary exponential functions to yield antagonistic (push-pull) firing rates (middle) for excitatory (ganglion cell, red) and inhibitory (interneuron, blue) inputs; input spike trains (right, rastergrams showing 100 trials) were generated as inhomogeneous Poisson processes. **(b)** Simulated membrane potential for control (black), altered excitation (green) and altered inhibition (purple). Dark-colored traces depict a single trial with nine additional trials in light gray. **(c)** Rastergrams for 100 trials depict spikes of the modeled relay cell for the three cases. Scale bar applies to **b** and **c**. **(d)** Information rate density plotted as a function of timescale for the three cases. The ordinate represents the negative derivative of the information rate,  $I(\tau)$ , with respect to  $\tau$ . **(e)** Estimated information rate for the three cases. Error bars in **f** represent s.d.



ganglion cells. This ON interneuron receives additional retinal input from an OFF ganglion cell that also synapses with a dendrite of an OFF interneuron. Furthermore, the ON interneuron is postsynaptic to the dendrite of that OFF interneuron, (see **Supplementary Fig. 1b**). Thus, each time the OFF ganglion cell fires, it produces a monosynaptic EPSC (in the ON interneuron) that is truncated by a disynaptic IPSC fed forward from the OFF interneuron, yielding waveforms like those we recorded (**Fig. 5b**).

Of course, other patterns of connectivity could build the pull in interneurons. The notches that precede IPSCs might come from strong intrinsic repolarizing currents<sup>46</sup>, dendritic spikelets<sup>47</sup> or electrically coupled cells<sup>48</sup>. The IPSCs might be generated by axonal connections from multiple interneurons or, although unlikely<sup>12,17</sup>, sign-inverting retinal synapses onto interneurons. It is doubtful that the pull comes from neurons in the perigeniculate nucleus. These cells provide weak, if any, input to local interneurons<sup>44</sup> and do not have receptive fields with a center-surround structure<sup>39</sup>.

### Shapes of synaptic inputs and the relay of information

Relay cells fire action potentials that lock to retinal input with millisecond fidelity<sup>23,26,39</sup>; presumably, such tight coupling is facilitated by the large and discrete shapes of retinogeniculate EPSPs. This temporal precision is important because spike timing is critical for encoding sensory information<sup>26,49</sup>. Our simulations support these conclusions, showing that jagged excitation is optimal for conveying information at fine timescales. Why should the pull signal in interneurons retain the high-frequency component of retinal spike trains? Perhaps the reason is to disinhibit relay cells on the timescale of single EPSPs and preserve the temporal structure of retinal input.

Several different mechanisms might generate the smooth, or low-passed, profiles that we recorded from interneurons and relay cells. The push signal in interneurons is probably blurred by the regenerative currents<sup>12</sup> engaged by retinal input. This form of synaptic integration might decouple the timings of pre- and postsynaptic spikes.

Past work supports this idea. Cross-correlations made from spike trains of simultaneously recorded ganglion cells and putative interneurons are broader than those made for ganglion cells and relay cells<sup>39</sup>. Thus, it is reasonable to hypothesize that convergent inhibitory inputs to a relay cell would arrive asynchronously and average to form a smooth pull signal; dendrodendritic input, if present, might be graded. What role might this low-passed inhibition serve? Our simulations show that smooth versus jagged inhibition has a greater effect on the postsynaptic relay cell's firing rate and increases the amount of information that each spike carries to cortex.

### METHODS

Methods and any associated references are available in the online version of the paper at <http://www.nature.com/natureneuroscience/>.

*Note: Supplementary information is available on the Nature Neuroscience website.*

### ACKNOWLEDGMENTS

We are grateful to L.M. Martinez for discussions throughout the project and thank Q. Wang for custom software. J. Provost, S.X.X. Xing, B. Gary, M. Bathen and M. Gerstmar reconstructed labeled cells, and M. Gerstmar also assisted with event sorting. This work was supported by the US National Institutes of Health (EY09593, J.A.H.), the Redwood Center for Theoretical Neuroscience (F.T.S.) and the National Science Foundation (IIS-0713657, F.T.S.).

### AUTHOR CONTRIBUTIONS

X.W. and J.A.H. performed the experiments with help from V.V. and C.S.S. X.W., J.A.H. and F.T.S. contributed to various analyses, and X.W. and F.T.S. developed the simulations. X.W., J.A.H. and F.T.S. wrote the manuscript, and X.W. prepared all of the figures.

## COMPETING FINANCIAL INTERESTS

The authors declare no competing financial interests.

Published online at <http://www.nature.com/natureneuroscience/>.

Reprints and permissions information is available online at <http://www.nature.com/reprintsandpermissions/>.

- Bickford, M.E. *et al.* Synaptic organization of thalamocortical axon collaterals in the perigeniculate nucleus and dorsal lateral geniculate nucleus. *J. Comp. Neurol.* **508**, 264–285 (2008).
- Montero, V.M. A quantitative study of synaptic contacts on interneurons and relay cells of the cat lateral geniculate nucleus. *Exp. Brain Res.* **86**, 257–270 (1991).
- Van Horn, S.C., Erisir, A. & Sherman, S.M. Relative distribution of synapses in the A-laminae of the lateral geniculate nucleus of the cat. *J. Comp. Neurol.* **416**, 509–520 (2000).
- Hubel, D.H. & Wiesel, T.N. Integrative action in the cat's lateral geniculate body. *J. Physiol. (Lond.)* **155**, 385–398 (1961).
- Wang, X. *et al.* Feedforward excitation and inhibition evoke dual modes of firing in the cat's visual thalamus during naturalistic viewing. *Neuron* **55**, 465–478 (2007).
- Denning, K.S. & Reinagel, P. Visual control of burst priming in the anesthetized lateral geniculate nucleus. *J. Neurosci.* **25**, 3531–3538 (2005).
- Martinez, L.M. *et al.* Receptive field structure varies with layer in the primary visual cortex. *Nat. Neurosci.* **8**, 372–379 (2005).
- Hamos, J.E., Van Horn, S.C., Raczkowski, D., Uhlrich, D.J. & Sherman, S.M. Synaptic connectivity of a local circuit neuron in lateral geniculate nucleus of the cat. *Nature* **317**, 618–621 (1985).
- Dan, Y., Atick, J.J. & Reid, R.C. Efficient coding of natural scenes in the lateral geniculate nucleus: experimental test of a computational theory. *J. Neurosci.* **16**, 3351–3362 (1996).
- Hirsch, J.A. *et al.* Functionally distinct inhibitory neurons at the first stage of visual cortical processing. *Nat. Neurosci.* **6**, 1300–1308 (2003).
- Hirsch, J.A., Alonso, J.M., Reid, R.C. & Martinez, L.M. Synaptic integration in striate cortical simple cells. *J. Neurosci.* **18**, 9517–9528 (1998).
- Acuna-Goycolea, C., Brenowitz, S.D. & Regehr, W.G. Active dendritic conductances dynamically regulate GABA release from thalamic interneurons. *Neuron* **57**, 420–431 (2008).
- Güllery, R.W. A quantitative study of synaptic interconnections in the dorsal lateral geniculate nucleus of the cat. *Z. Zellforsch. Mikrosk. Anat.* **96**, 39–48 (1969).
- Coomes, D.L., Bickford, M.E. & Schofield, B.R. GABAergic circuitry in the dorsal division of the cat medial geniculate nucleus. *J. Comp. Neurol.* **453**, 45–56 (2002).
- Godwin, D.W. *et al.* Ultrastructural localization suggests that retinal and cortical inputs access different metabotropic glutamate receptors in the lateral geniculate nucleus. *J. Neurosci.* **16**, 8181–8192 (1996).
- Montero, V.M. Localization of gamma-aminobutyric acid (GABA) in type 3 cells and demonstration of their source to F2 terminals in the cat lateral geniculate nucleus: a Golgi-electron-microscopic GABA-immunocytochemical study. *J. Comp. Neurol.* **254**, 228–245 (1986).
- Govindaiah, G. & Cox, C.L. Metabotropic glutamate receptors differentially regulate GABAergic inhibition in thalamus. *J. Neurosci.* **26**, 13443–13453 (2006).
- Wilson, J.R., Forestner, D.M. & Cramer, R.P. Quantitative analyses of synaptic contacts of interneurons in the dorsal lateral geniculate nucleus of the squirrel monkey. *Vis. Neurosci.* **13**, 1129–1142 (1996).
- Friedlander, M.J., Lin, C.S., Stanford, L.R. & Sherman, S.M. Morphology of functionally identified neurons in lateral geniculate nucleus of the cat. *J. Neurophysiol.* **46**, 80–129 (1981).
- Humphrey, A.L. & Weller, R.E. Structural correlates of functionally distinct X-cells in the lateral geniculate nucleus of the cat. *J. Comp. Neurol.* **268**, 448–468 (1988).
- Sherman, S.M. & Friedlander, M.J. Identification of X versus Y properties for interneurons in the A-laminae of the cat's lateral geniculate nucleus. *Exp. Brain Res.* **73**, 384–392 (1988).
- Levick, W.R., Cleland, B.G. & Dubin, M.W. Lateral geniculate neurons of cat: retinal inputs and physiology. *Invest. Ophthalmol.* **11**, 302–311 (1972).
- Usrey, W.M., Reppas, J.B. & Reid, R.C. Specificity and strength of retinogeniculate connections. *J. Neurophysiol.* **82**, 3527–3540 (1999).
- Schwartz, O., Pillow, J.W., Rust, N.C. & Simoncelli, E.P. Spike-triggered neural characterization. *J. Vis.* **6**, 484–507 (2006).
- Mante, V., Bonin, V. & Carandini, M. Functional mechanisms shaping lateral geniculate responses to artificial and natural stimuli. *Neuron* **58**, 625–638 (2008).
- Koepsell, K. *et al.* Retinal oscillations carry visual information to cortex. *Front. Sys. Neurosci.* **3** (2009).
- Blitz, D.M. & Regehr, W.G. Timing and specificity of feed-forward inhibition within the LGN. *Neuron* **45**, 917–928 (2005).
- Granseth, B. & Lindstrom, S. Unitary EPSCs of corticogeniculate fibers in the rat dorsal lateral geniculate nucleus *in vitro*. *J. Neurophysiol.* **89**, 2952–2960 (2003).
- Pape, H.C. & McCormick, D.A. Electrophysiological and pharmacological properties of interneurons in the cat dorsal lateral geniculate nucleus. *Neuroscience* **68**, 1105–1125 (1995).
- Frishman, L.J. & Levine, M.W. Statistics of the maintained discharge of cat retinal ganglion cells. *J. Physiol. (Lond.)* **339**, 475–494 (1983).
- Bullier, J. & Norton, T.T. Comparison of receptive-field properties of X and Y ganglion cells with X and Y lateral geniculate cells in the cat. *J. Neurophysiol.* **42**, 274–291 (1979).
- Gilbert, C.D. Laminar differences in receptive field properties of cells in cat primary visual cortex. *J. Physiol. (Lond.)* **268**, 391–421 (1977).
- Mastrorade, D.N. Nonlagged relay cells and interneurons in the cat lateral geniculate nucleus: receptive-field properties and retinal inputs. *Vis. Neurosci.* **8**, 407–441 (1992).
- Fitzpatrick, D., Penny, G.R. & Schmechel, D.E. Glutamic acid decarboxylase-immunoreactive neurons and terminals in the lateral geniculate nucleus of the cat. *J. Neurosci.* **4**, 1809–1829 (1984).
- Destexhe, A., Neubig, M., Ulrich, D. & Huguenard, J. Dendritic low-threshold calcium currents in thalamic relay cells. *J. Neurosci.* **18**, 3574–3588 (1998).
- Blitz, D.M. & Regehr, W.G. Retinogeniculate synaptic properties controlling spike number and timing in relay neurons. *J. Neurophysiol.* **90**, 2438–2450 (2003).
- Hirsch, J.C. & Burnod, Y. A synaptically evoked late hyperpolarization in the rat dorsolateral geniculate neurons *in vitro*. *Neuroscience* **23**, 457–468 (1987).
- Wilson, J.R. Synaptic organization of individual neurons in the macaque lateral geniculate nucleus. *J. Neurosci.* **9**, 2931–2953 (1989).
- Dubin, M.W. & Cleland, B.G. Organization of visual inputs to interneurons of lateral geniculate nucleus of the cat. *J. Neurophysiol.* **40**, 410–427 (1977).
- Datskovskaia, A., Carden, W.B. & Bickford, M.E. Y retinal terminals contact interneurons in the cat dorsal lateral geniculate nucleus. *J. Comp. Neurol.* **430**, 85–100 (2001).
- Bloomfield, S.A. & Sherman, S.M. Dendritic current flow in relay cells and interneurons of the cat's lateral geniculate nucleus. *Proc. Natl. Acad. Sci. USA* **86**, 3911–3914 (1989).
- Cox, C.L., Reichova, I. & Sherman, S.M. Functional synaptic contacts by intranuclear axon collaterals of thalamic relay neurons. *J. Neurosci.* **23**, 7642–7646 (2003).
- Lörincz, M.L., Kekesi, K.A., Juhasz, G., Crunelli, V. & Hughes, S.W. Temporal framing of thalamic relay-mode firing by phasic inhibition during the alpha rhythm. *Neuron* **63**, 683–696 (2009).
- Cucchiari, J.B., Uhlrich, D.J. & Sherman, S.M. Electron-microscopic analysis of synaptic input from the perigeniculate nucleus to the A-laminae of the lateral geniculate nucleus in cats. *J. Comp. Neurol.* **310**, 316–336 (1991).
- Pasik, P., Pasik, T. & Hámori, J. Synapses between interneurons in the lateral geniculate nucleus of monkeys. *Exp. Brain Res.* **25**, 1–13 (1976).
- Person, A.L. & Perkel, D.J. Unitary IPSPs drive precise thalamic spiking in a circuit required for learning. *Neuron* **46**, 129–140 (2005).
- Contreras, D., Curro Dossi, R. & Steriade, M. Electrophysiological properties of cat reticular thalamic neurones *in vivo*. *J. Physiol. (Lond.)* **470**, 273–294 (1993).
- Landisman, C.E. *et al.* Electrical synapses in the thalamic reticular nucleus. *J. Neurosci.* **22**, 1002–1009 (2002).
- Butts, D.A. *et al.* Temporal precision in the neural code and the timescales of natural vision. *Nature* **449**, 92–95 (2007).

## ONLINE METHODS

**Preparation.** Adult female cats (1.5–3.5 kg) were prepared as described previously<sup>5</sup>. Anesthesia was induced with propofol and sufentanil (20 mg per kg + 1.5 µg per kg, intravenous) and maintained with propofol and sufentanil (5 µg per kg per h + 1.5 µg per kg per h, intravenous). All procedures adhered to the guidelines of the US National Institutes of Health and the Institutional Animal Care and Use Committee of the University of Southern California.

**Stimulation.** Discs, annuli and natural movies were displayed at 19–50 frames per s on a computer monitor (refresh rate, 144–160 Hz) by means of a stimulus generator (Vsg2/5 or ViSaGe, Cambridge Research Design) as described previously<sup>5</sup>. We also used two-dimensional Gaussian white noise at 33% contrast with a spatial resolution of 0.5 or 1 degree (luminance values below 0 and above 2 × mean were truncated); one stimulus trial typically included 16,384 frames, updated at 48 Hz with a video refresh of 144 Hz.

**Recordings.** Whole-cell recordings with dye-filled pipettes were made using standard techniques<sup>10</sup>, except that we often used electrodes with resistances >20 MΩ to improve chances of recording from small cells. Signals were recorded with an Axopatch 200A amplifier (Axon Instruments), digitized at 10–20 kHz (Power1401 data acquisition system, Cambridge Electronic Design) and stored for further analysis. It was often impractical to assign absolute resting voltage, as the ratio of access to seal resistance led to a voltage division in the neural signal<sup>11</sup>. Unless otherwise noted, all recordings were made above the reversal potential for inhibition and below the threshold for firing. The integrity of the recordings was monitored by responses to current injection.

**Anatomical analysis.** Following histological processing<sup>10</sup>, cells were identified as interneurons (Guillery type III cells<sup>50</sup>) using standard criteria<sup>19–21,29,41,50</sup>, such as complicated and often thin dendrites, appendages on distal processes, and small somas (Supplementary Fig. 2). Different classes of relay cells were also distinguished on the basis of various anatomical characteristics, such as somal size, shape of the dendritic arbor and the presence of grape-like appendages on primary dendrites<sup>19,20</sup>. Some cells were reconstructed in three dimensions using a NeuroLucida System (MicroBrightfield).

**Receptive fields and linear-nonlinear models.** Standard methods of reverse correlation<sup>24</sup> were used to compute the spatiotemporal receptive fields except that the continuous membrane current (from which action currents were removed<sup>5</sup>) was substituted for traditional, discrete spike times, as follows. First the stimulus was rewritten as a two dimensional matrix,  $S$ , of size  $m \times n$ , where  $m$  is the number of time bins and  $n$  is the number of pixels in the receptive field. The receptive field was then  $k = (S^T S)^{-1} S^T r$ , where  $r$  is the continuous response signal of size  $m \times 1$ . If the stimulus is white noise, as in our experiments, its autocorrelation will be identity and the receptive field can be computed simply by reverse correlation  $k = (S^T r)$ .

We computed the spatiotemporal receptive fields from 15/16 (15,360 frames) of the Gaussian white noise sequence and used these as the linear component of the model (the remaining 1/16 (1,024 frames) was reserved to assess the performance of the model). The time bin, or temporal resolution (20.8 ms), was set by the rate of stimulus update (48 Hz). The static nonlinearity function was estimated by fitting (least mean square) the intracellular response to the output of the spatiotemporal receptive field. The shape of the nonlinearity for interneurons

and relay cells was captured by a sigmoid function  $f(x) = \frac{a}{1 + e^{b(x-c)}}$ , which

takes into account slight saturation and thresholding of the response. When a linear function was substituted for the sigmoid, the prediction of the model was only slightly worse, less than 3%; thus, this choice of parameterization did not appreciably influence the performance of the model. Finally, the performance of the model was assessed by cross-validation (using the reserved 1/16 of the data) and quantified as the explained variance in the response that the model predicted (because the data did not contain multiple trials of the same stimulus, the percentage of explained variance was calculated with respect to the total variance in the signal).

**Deflection index.** To capture asymmetric structures in the direction, or sign, of the membrane trajectory across various timescales, we devised an index that reflects the dominance of inward versus outward deflections in the intracellular signal (see Supplementary Fig. 3). First, we differentiated the recordings of the membrane current  $I(t)$  (from which action currents had been removed, see ref. 5) at different time scales,  $\tau$ . The resulting differentiated signals were

$$i(t; \tau) = \frac{1}{\tau} \left( I \left( t + \frac{\tau}{2} \right) - I \left( t - \frac{\tau}{2} \right) \right)$$

We then formed distributions of the differentiated signals (that is, the change in membrane current at a given timescale) and computed the deflection indices  $\gamma_1(\tau)$  as the skewness of these distributions

$$\gamma_1(\tau) = m_3(\tau) [m_2(\tau)]^{-3/2}$$

Here,  $m_2(\tau)$  and  $m_3(\tau)$  are the second and third central moments of the distribution of  $i(t; \tau)$ . To characterize the asymmetry of deflection across all time scales, we normalized the deflection indices and performed principal component analysis on the normalized index  $\gamma$  as a function of time scales for the population ( $n = 119$ ).

**Event sorting and counting.** Intracellular, voltage-damped recordings were filtered digitally (Gaussian filter, 0.5-ms bandwidth) and then differentiated twice. Potential neural events, spikes and unitary synaptic currents, were detected as concave local minima (zero crossing of the first derivative with a negative second derivative). Neural events were clustered using commercial software (Spike2, Cambridge Electronic Design).

**Exponential leaky integrate-and-fire model.** Time evolution of membrane potential ( $V_m$ ) and synaptic conductances ( $g_E$  and  $g_I$ ) of the modeled relay cell were defined as follows:

$$C_m \frac{dV_m}{dt} = g_L \Delta_T e^{-\Delta_T} \frac{V_m - V_T}{\Delta_T} - g_L(V_m - E_L) - g_E(V_m - E_E) - g_I(V_m - E_I)$$

$$\tau_E \frac{dg_E}{dt} = -g_E$$

$$\tau_I \frac{dg_I}{dt} = -g_I$$

where  $C_m = 1 \mu\text{F cm}^{-2}$ ,  $g_L = 40 \mu\text{S cm}^{-2}$ ,  $\Delta_T = 2 \text{ ms}$ ,  $V_T = -50 \text{ mV}$ ,  $E_L = -60 \text{ mV}$ ,  $E_E = 0 \text{ mV}$ ,  $E_I = -80 \text{ mV}$ ,  $\tau_E = 1.5 \text{ ms}$  and  $\tau_I = 10 \text{ ms}$ . The modeled relay cell received input from a single ganglion cell and four inhibitory interneurons. Each retinal spike triggered an increase in synaptic conductance by  $g_{Em} = 200 \mu\text{S cm}^{-2}$  or  $g_{Im} = 12.5 \mu\text{S cm}^{-2}$ . When the membrane potential reached  $V_\theta = 0 \text{ mV}$ , a spike was fired and the membrane potential returned to  $V_{\text{reset}} = -70 \text{ mV}$ .

The spike trains of the inputs to the relay cell (that is, the ganglion cell and interneurons) were modeled as inhomogeneous Poisson processes that encoded a pink noise signal for which the power was scaled to  $1/f$  for frequencies >0.5 Hz. Instantaneous firing rates were generated by passing the signal through complementary, inverse (push-pull) exponential nonlinearities. Average firing rates for both types of input were 30 spikes per s and the mean firing rate for relay cells was nearly 10 spikes per s, corresponding to 30–40% efficacy. To model smooth excitation, we increased to  $\tau_E = 10 \text{ ms}$  and reduced  $\bar{g}_E$  proportionately. To model jagged inhibition, we reduced the number of presynaptic interneurons from four to only one and scaled  $\bar{g}_I$  proportionately. Simulations made with all three models were done using 32768 repeats of trials of duration,  $T = 20 \text{ s}$  and sampled at 10 kHz.

Information rates for the thalamic spike trains were estimated at different time scales ( $\tau$ )

$$I(\tau) = \sum_{t=1}^T \frac{\tau}{T} r(t) \log_2 \frac{r(t)}{\bar{r}}$$



where  $r(t)$  was the firing rate of the  $t$ th time bin and  $\bar{r}$  the mean firing rate.

Information rate density was then defined as  $i(\tau) = -\frac{dI(\tau)}{d\tau}$ , which is the sensitivity of information rate with respect to the time scale at which the firing rate was measured. The total information rate was estimated by extrapolating the timescale to zero:  $I = \lim_{\tau \rightarrow 0} I(\tau)$ .

**Predicting anatomical class on the basis of physiology.** We assessed how well the physiological profile recorded from a given neuron predicted its anatomical class, based on the 36 cases ( $k = 36$ ) for which both physiological and anatomical data were available for the same cell. The accuracy of the match between the anatomical and physiological classification of interneurons ( $I$ ) and relay cells ( $R$ ) is given by the conditional probabilities  $\alpha = p(I_{\text{phys}}|I_{\text{anat}})$  and  $\beta = p(R_{\text{phys}}|R_{\text{anat}})$ , respectively.

To estimate the importance of our particular result, we made two assumptions based on the observation that both the anatomical and physiological classifier yielded the same approximate ratio of two cell types (corresponding to the distribution of relay cells and interneurons reported previously). Specifically, we assumed the ratio of interneurons to relay cells is 1:4 and that the conditional probabilities preserved this ratio. For any given  $\beta$ , these assumptions set  $\alpha$  to

$$\alpha = \frac{(1-p)\beta + 2p - 1}{p}$$

The probability of obtaining the experimental results that we observed is

$$P_0 = \alpha^{kp} \beta^{k(1-p)} = \beta^k \left( \frac{(1-p)\beta + 2p - 1}{\beta p} \right)^{kp}$$

By way of example, if the correspondence between both classifiers were perfect, not just for our small sample, but for any sample size, then  $\alpha = \beta = 1$  and the probability of obtaining our experimental result would be certain,  $P_0 = 1$ .

If we assumed that the physiological classifier randomly assigned anatomical type while preserving the 1:4 ratio,  $p$ , of interneurons to relay cells, then  $\alpha = 1 - \beta = \frac{1}{4}$ . In this case, the probability that we would have found the empiri-

cally observed perfect correspondence between physiology and anatomy by chance is extremely low,  $P_0 = 10^{-9}$ .

Next, rather than estimating the probability of arriving at our empirical result by chance (as above), we specifically asked how faithfully the physiological classifier predicts anatomical type. Thus, we set  $P_0 = 0.05$  and calculated the corresponding values for the conditional probabilities  $\alpha$  and  $\beta$ . The resulting values were  $\alpha = 0.88$  and  $\beta = 0.95$ , indicating that even conditional probabilities this close to 1 would yield only an insignificant result. Thus, the actual values for  $\alpha$  and  $\beta$  must be much larger. In sum, this analysis suggested that the physiology predicted the anatomy with very high fidelity.

50. Guillery, R.W. A study of Golgi preparations from the dorsal lateral geniculate nucleus of the adult cat. *J. Comp. Neurol.* **128**, 21–50 (1966).